Eur. Phys. J. E (2018) **41**: 141
DOI 10.1140/epje/i2018-11750-4

THE EUROPEAN PHYSICAL JOURNAL E

Regular Article

Nematic liquid crystals of bifunctional patchy spheres*

Khanh Thuy Nguyen and Cristiano De Michele[a]

Dipartimento di Fisica, "Sapienza" Università di Roma, P.le A. Moro 2, 00185 Roma, Italy

Received 2 July 2018 and Received in final form 22 October 2018
Published online: 6 December 2018

Abstract. Anisotropic interactions can bring about the formation, through self-assembly, of semi-flexible chains, which in turn can give rise to nematic phases for suitable temperatures and concentrations. A minimalist model constituted of hard cylinders decorated with attractive sites has been already extensively studied numerically. Simulation data shows that a theoretical approach recently proposed is able to properly capture the physical properties of these self-assembly–driven liquid crystals. Here, we investigated a simpler model constituted of bifunctional Kern-Frenkel hard spheres which does not possess steric anisotropy but which can undergo a istropic-nematic transition as a result of their self-assembly into semi-flexible chains. For this model we compare an accurate numerical estimate of isotropic-nematic phase boundaries with theoretical predictions. The theoretical treatment, originally proposed for cylinder-like particles, has been greatly simplified and its predictions are in good agreement with numerical results. Finally, we also assess a crucial, and not obvious, hypothesis used in the theory, *i.e.* the ability of the Onsager trial function to properly model particle orientation in the presence of aggregation, that has not been properly checked yet.

1 Introduction

Self-assembly, *i.e.* the reversible aggregation of basic building blocks, plays a central role in material science, soft-matter and biophysics [1–3]. In particular, in many systems, such as micelles [4–6], fibers and fibrils [7–10], aqueous solutions of short (nano) [11–13] and long B-DNA [14–17], G-quadruplexes [18], chromonics [19–23], and colloidal polymers [24], linear semi-flexible chains form as a result of reversible aggregation. This ensemble of semi-flexible chains, if sufficiently concentrated, can undergo a transition from an isotropic to a self-assembly–driven nematic phase and by further increasing the concentration to other liquid-crystalline phases [7, 11, 25, 26]. To gain some insight into the physical mechanisms behind the formation of these lyotropic liquid crystals as a result of self-assembly of their constituent particles, several theoretical approaches have been proposed in the past [5, 27–32]. In all these studies the crucial role of polydispersity, particle shape and chain flexibility unambiguously emerges. In ref. [33] self-assembling patchy hard cylinders —intended as a minimalist modeling of self-assembly–driven liquid crystals of particles with anisotropic shape— have been studied and compared to a theoretical approach which has been proposed by one of the two authors of the present manuscript [31]. Bent hard cylinders have been also investigated in ref. [34], where the degree of bending plays the role of an effective persistence-length and theoretical predictions, that have been made by using the same aforementioned approach, nicely match numerical data. These studies elucidated how the physical properties of these systems can be related to polydispersity, particles shape and chain flexibility. Here, we investigate an even simpler system, *i.e.* hard spheres decorated with attractive interaction sites according to the Kern-Frenkel (KF) model [35]. The physical properties of bifunctional patchy spheres in the isotropic phase have already been fully understood both theoretically [36–39] and numerically [40–42], anyway a careful study of the isotropic-nematic (IN) transition has been attempted only for very stiff chains of bifunctional spheres [28, 29] and in latter studies numerical results were compared with a semi-phenomenological theoretical approach which was not able to capture some peculiar features of self-assembly–driven liquid crystals [33]. The present model is more reminiscent of reversible polymers than chromonic liquid crystals, such as those obtained from DNA duplexes, fibrils, dyes (SSY or DCSG) or G-quadruplexes, because the aggregating units have no shape anisotropy. Hence, it is not obvious whether the theory, which reproduces numerical data and experiments for cylinder-like and disk-like particles [31, 33, 43, 44], can still offer a valid description of the present system. For example, in ref. [45] it is shown

* Supplementary material in the form of a .pdf file available from the Journal web page at
https://doi.org/10.1140/epje/i2018-11750-4

[a] e-mail: cristiano.demichele@uniroma1.it

that the Parson-Lee decoupling approximation, which is exploited also in the theory developed in ref. [31], does not provide a good description of the IN phase transition for linear tangent hard-sphere chains (LTHSCs) comprising 7 tangentially bonded segments. A further motivation for studying both numerically and theoretically the phase diagram of bifunctional patchy spheres can be rooted in the fact that the design of bifunctional colloidal particles of spherical shape, which can self-assemble into semiflexible reversible polymers and thus give rise to nematic liquid crystals, is surely not out of reach in the next future [46–54]. With this work we aim to provide predictions and guidance for these possible future experimental studies.

We will show that, despite its simplicity and the lack of shape anisotropy of aggregating monomers, this system can still undergo an IN transition, whose phase boundaries exhibits a clear reentrant behavior in the phase diagram as already observed in bifunctional hard cylinders, DNA duplexes and chromonics [31, 33, 44, 55]. Moreover, the theoretical treatment, which is used in the present work, although greatly simplified with respect to the ones used in previous studied, proved to be in good agreement with numerical results. On top of this we provide in this work a careful check of an important hypothesis used in the theory, *i.e.* the assumption that the orientational distribution of monomers can be drawn from the Onsager trial function [56], which is a valid modeling of the orientational distribution of non-aggregating anisotropic particles [57, 58]. This hypothesis, although rather reasonable, has not been directly verified in these systems yet.

The manuscript is organized as detailed in the following. In sect. 2 we describe the model which we used in the Monte Carlo (MC) simulation and we provide some details of the theory. We also discuss the numerical techniques used to trace the phase boundaries of the isotropic-nematic transition. In sect. 3 we show the results obtained from computer simulations in comparison with theoretical predictions. Finally, in sect. 4 the conclusions will be drawn.

2 Methods

2.1 Model

In this paper we study hard spheres of diameter D decorated with 2 attractive sites (also called "sticky patches") as illustrated in fig. 1. These attractive sites on particles 1 and 2 interact via a KF potential [35]:

$$V_{KF}(\mathbf{r}) = \begin{cases} -u_0, & \text{if} \begin{cases} D < r < D+\delta & \text{and} \\ \cos(\theta_1) > \cos(\theta_{max}) & \text{and} \\ -\cos(\theta_2) > \cos(\theta_{max}), \end{cases} \\ 0, & \text{otherwise,} \end{cases} \tag{1}$$

where θ_1 and θ_2 are the angles between the directions of the site on particle 1 and 2, respectively, and vector $\mathbf{r}$ points from the center of particle 1 to that of particle 2; δ and θ_{max} are the parameters of the potential that are explained in fig. 1(b). One can enforce the rule of no more than 1 bond per patch by imposing the following condition on the angle θ_{max} for a particular value of δ:

$$\sin(\theta_{max}) \leq [2(1+\delta/D)]^{-1}. \tag{2}$$

A nice feature of the KF interaction potential is that it offers the flexibility to adjust bonding volume and persistence length independently. To study the isotropic-nematic transition we set $\delta = 0.546D$ and $\cos(\theta_{max}) = 0.9462$, which results in maximum bonding volume and in a persistence length $l_p = 18.35$ in monomers unit.

In eq. (1) u_0 is the binding energy and in the following we will make use of the adimensional temperature $T^* = k_BT/u_0$, where k_B is the Boltzmann constant. Here, as in previous studies on self-assembly–driven liquid crystals, u_0 does not depend on the aggregate size, *i.e.* the self-assembly process is assumed to be isodesmic [59, 60].

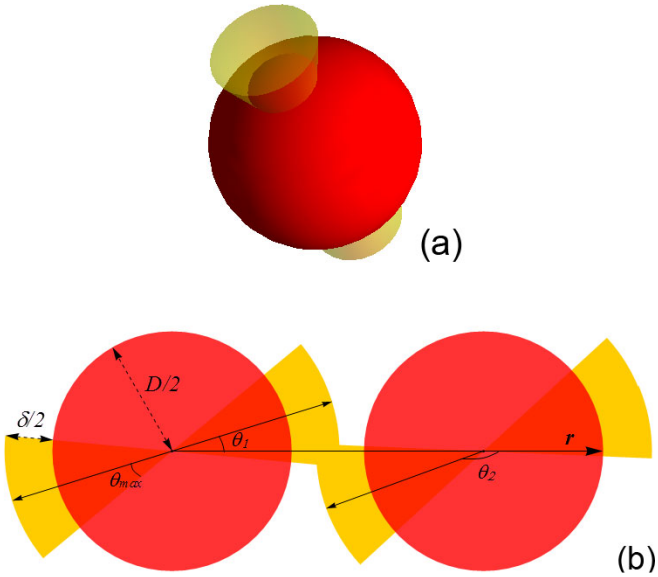

Fig. 1. The model of hard spheres with KF patches. (a) Illustration of a particle and its KF patches. (b) In 2D, an example of 2 bonded particles with explanations of the parameters of the model; note that the two bonding patches (yellow spherical truncated cones) overlap and the vector $\mathbf{r}$, joining the centers of 2 particles, crosses both caps.

2.2 Monte Carlo simulations

We use the Kofke thermodynamics integration (KI) [61–63] to build coexistence lines over a quite wide range of temperatures. The KI method is based on the numerical integration of the Clausius-Clapeyron (CC) differential equation, *i.e.*

$$\left(\frac{\mathrm{d}\ln P}{\mathrm{d}\beta}\right)\bigg|_{coex} = -\frac{\Delta h}{\beta P \Delta v}, \tag{3}$$

where P is the pressure of the system, Δh is the enthalpy per particle difference between the two phases, and Δv is

their volume per particle difference. For each integration step over $\beta = 1/k_BT$, two separate Monte Carlo (MC) simulations in the NPT ensemble are carried out for the two coexisting phases, from which an estimate of Δh and Δv and thus of a new value of pressure P at coexistence is obtained (see the Electronic Supplementary Material (ESM) for further details on the method). For NPT MC simulations we used $N = 6000$ particles and we numerically integrate over temperature the CC equation starting from $T^* = 0.130$ up to $T^* = 0.165$ and down to $T^* = 0.12$. The integration of the CC differential equation in eq. (3) requires giving some initial condition, *i.e.* an initial estimate of coexistence densities at a given temperature. These initial coexistence densities have been estimated by successive umbrella sampling (SUS) MC simulations carried out at $T^* = 0.130$.

The SUS method provides a convenient way to efficiently calculate $P(N)$, *i.e.* the probability $P(N)$ of finding N particles at fixed volume, temperature and chemical potential, *i.e.* in the grand-canonical (GC) ensemble [64, 65]. Within the SUS approach the investigated range of particles is partitioned into several overlapping regions and for each of them an independent GC-MC simulation is performed in parallel with the others. In our GC-MC simulations the number of particles varies between 4500 and 7380 (see the ESM for more details). The entire $P(N)$ distribution can be conveniently reconstructed by matching the overlapping of distributions gathered from all the GC-MC simulations running in parallel. A standard histogram reweighting technique can be exploited to enforce an equal-area condition below the $P(N)$ peaks associated to the isotropic and nematic coexisting phases, thus obtaining the $P(N)$ at coexistence. Finally, the coexistence densities can be evaluated by calculating the average number of particles below the two peaks associated to the two coexisting phases. As suggested in ref. [65] we employed an elongated (*i.e.* not cubic) simulation box of volume $V = L_xL_yL_z$ with $L_y = L_z = 16D$ and $L_x = 40D$. Simulation box dimensions have been chosen to satisfy the following conditions:

$$L_x \gg L_y \quad \text{and} \quad L_x \gg L_z, \tag{4}$$

where the z-axis is parallel to the nematic director (to which all particles are aligned in the starting configuration used for the SUS simulation). The chosen shape of the simulation box ensures that the IN interface builds parallel to the yz-plane. The rationale of latter choice is extensively discussed in the ESM. When the system is nematic, the chains can get quite long and the box should be large enough to not affect anyhow the growth of long chains. Since L_z should fulfill the condition provided in eq. (4), $L_z \approx 15D$, one can accommodate in the box chain as long as 15-mers, which are still larger than the average chain length in all of the systems we studied with SUS. We performed two additional SUS simulations at $T^* = 0.12$ and $T^* = 0.155$ intended as checkpoints for KI as shown in fig. 3.

Starting from configurations obtained from KI we carried out a canonical NVT MC simulation along coexistence lines to obtain an accurate estimate of average lengths of chains M. For NVT MC simulations we employed $N = 6000$ particles. In these simulations for the I phase we used a cubic box while for the N phase an elongated box chosen according to eq. (4) has been used. Periodic boundary conditions in all directions have been used in all simulations.

2.3 Theory

As proposed in refs. [31, 33, 43] for polydisperse mixtures of self-assembled linear aggregates, if $\nu(l)$ is the number density of aggregates of length l, which obeys the normalization condition $\sum_l \nu(l) = \rho$, with $\rho = N/V$, the Helmholtz free energy F of the I and N phases is assumed to comprise the following contributions:

$$F = F^{id} + F^{excl} + F^{or} + F^{st}, \tag{5}$$

where F^{id} is the ideal gas free energy, F^{excl} accounts for the excluded-volume interactions, F^{or} quantifies the entropy decrease due to orientational order and the last term, F^{st}, is the stacking free energy which accounts for monomer aggregation and which is expressed in terms of $\Delta = \Delta(T)$, the bonding free energy [31]. Here, as in refs. [31, 55], $\nu(l)$ is assumed to be exponential, *i.e.* $\nu(l) = \rho M^{(l-1)}/(M-1)^{(l+1)}$, with M the average cluster length.

The F^{or} is expressed as the sum of two contributions which have been proposed for the limiting cases of stiff and very flexible rods [57] where their weight is controlled by an adimensional adjustable parameter l_0 which we fixed to the value of 16.

The excluded-volume contribution to the free energy, F^{excl} can be written in terms of $\nu(l)$ as follows:

$$\frac{\beta F_0^{excl}}{V} = \frac{\eta(\zeta\phi)}{2} \sum_l \sum_{l'} \nu(l)\nu(l')\overline{v}^{excl}(l,l'), \tag{6}$$

where $\overline{v}^{excl}(l,l')$ is the excluded volume between two aggregates made of l and l' disks, and $\eta(\zeta\phi)$ is a modified Parsons-Lee factor [66, 67], where the system volume fraction $\phi = \rho D^3\pi/6$ is scaled by a factor ζ. The latter modification of the Parson-Lee theory is based on the of the so-called effective molecular volume of non-convex hard bodies as suggested in ref. [68], where a system of linear fused hard sphere chains was studied. The value used for ζ in the theoretical calculations will be provided later. If $\mathbf{R}_1 = \{\mathbf{r}_{1,1} \dots \mathbf{r}_{1,l}\}$, $\mathbf{R}_2 = \{\mathbf{r}_{2,1} \dots \mathbf{r}_{2,l'}\}$, $\mathbf{U}_1 = \{\mathbf{u}_{1,1} \dots \mathbf{u}_{1,l}\}$ and $\mathbf{U}_2 = \{\mathbf{u}_{2,1} \dots \mathbf{u}_{2,l'}\}$, where $\mathbf{r}_{\gamma,i}$ and $\mathbf{u}_{\gamma,i}$ are the position and the orientation (unit vector) of monomer i belonging to the chain $\gamma = 1, 2$, the excluded volume v_{excl} of two chains 1 and 2 composed of l and l' monomers in the isotropic phase is defined as

$$\overline{v}_{iso}^{excl}(l,l') = -\frac{1}{16\pi^2 V^{l+l'-1}} \int' \mathrm{d}\mathbf{R}_1 \mathrm{d}\mathbf{R}_2 \, \mathrm{d}\boldsymbol{\Omega}_1 \mathrm{d}\boldsymbol{\Omega}_2 \times e_{12}^{ll'}(\mathbf{R}_1, \mathbf{U}_1, \mathbf{R}_2, \mathbf{U}_2), \tag{7}$$

where $\mathbf{u}_{\gamma,i}$ is the orientation of monomer i belonging to aggregate γ, $\mathrm{d}\mathbf{R}_\gamma = \prod_{i=1}^{l} \mathrm{d}\mathbf{r}_{\gamma,i}$, $\mathrm{d}\boldsymbol{\Omega}_\gamma = \prod_{i=1}^{l} \mathrm{d}\boldsymbol{\omega}_{\gamma,i}$ with $\mathrm{d}\boldsymbol{\omega}_{\gamma,i}$ the infinitesimal solid angle around the orientation $\mathbf{u}_{\gamma,i}$ and $e_{12}^{ll'}$ is the Mayer function [69]:

$$e_{12}^{ll'}(\mathbf{R}_1, \mathbf{U}_1, \mathbf{R}_2, \mathbf{U}_2) = \exp\{-U_h(\mathbf{R}_1, \mathbf{U}_1, \mathbf{R}_2, \mathbf{U}_2)/k_B T\} - 1, \tag{8}$$

with $U_h(\mathbf{R}_1, \mathbf{U}_1, \mathbf{R}_1, \mathbf{U}_2)$ being the hard-core pair potential:

$$U_h(\mathbf{R}_1, \mathbf{U}_1, \mathbf{R}_2, \mathbf{U}_2) = \begin{cases} \infty, & \text{if } 1,2 \text{ overlap,} \\ 0, & \text{if } 1,2 \text{ do not overlap.} \end{cases} \tag{9}$$

The prime sign in the integral of eq. (7) means that the domain of integration is restricted to the positions and orientations of monomers such that i) within each chain only two monomers are single bonded and all the remaining monomers (if any) are double bonded[1] and that ii) chains do not self-overlap.

In ref. [70] the excluded volume of two rigid LTHSCs both in the isotropic and nematic phase has been calculated analytically, here we use the same analytical form with some modifications to account for the finite range of the SW interaction between patches (*i.e.* the spheres are not touching each other as assumed in ref. [70] and the resulting chain is not rigid). In the isotropic phase for the theoretical calculations, we use the following form for the excluded volume:

$$\overline{v}_{iso}^{excl}(l, l') = (\xi_2 D)^3 \frac{\pi}{6} \left[\mathcal{K} \frac{\pi}{4} \xi_1^2 l l' + \left(11 - \mathcal{K}\frac{\pi}{2}\right) \times \xi_1 \frac{l + l'}{2} - 3 + \mathcal{K}\frac{\pi}{4} \right], \tag{10}$$

where $\mathcal{K} = 3.53390$. Equation (10) is the excluded volume in the isotropic phase of two LTHSCs of length $\xi_1 l$ and $\xi_1 l'$ and sphere diameter equal to $\xi_2 D$ [70]. The only adjustable parameters in eq. (10) are ξ_1 and ξ_2 that account for the fact that, because of the finite range of SW interaction between patches, given a chain of l KF spheres, the length and diameter of an equivalent LTHSC comprises $\xi_1 l$ spheres of diameter $\xi_2 D$. In passing we note that, since the expression for the excluded volume in eq. (10) is a second-order polynomial in l and l', the scaling behavior with respect to the chain length is identical to the one assumed and discussed in ref. [31], where one can identify three contributions which come from end-end, end midsection and midsection-midsection steric interactions between two chains. Within the present approach for the calculation of the excluded-volume contribution to the free energy, a chain $\mathcal{C}_D$ comprising l spheres of diameter D is mapped onto an equivalent chain $\mathcal{C}_\xi$ of $\xi_1 l$ spheres of diameter $\xi_2 D$. Since the ratio between the volume of $\mathcal{C}_\xi$ and $\mathcal{C}_D$ amounts to $\xi_1 \xi_2^3$, we have to consistently set $\zeta = \xi_1 \xi_2^3$ in eq. (6). The numerical procedure to estimate ξ_1 and ξ_2 includes first the evaluation of the excluded volume in eq. (7) for $l = 1, \ldots, 10$ via Monte Carlo integration; then eq. (10) is fit to these data, using ξ_1 and ξ_2 as fitting parameters.

Similarly, in the nematic phase we assume [31]:

$$\overline{v}_{nem}^{excl}(l, l') = (\xi_2 D)^3 \frac{\pi}{6} \Big\{ \mathcal{K} B_n(\alpha) \xi_1^2 l l' + [11 - 2\mathcal{K} B_n(\alpha)] \times \xi_1 \frac{l + l'}{2} - 3 + \mathcal{K} B_n(\alpha) \Big\}, \tag{11}$$

where $B_n(\alpha)$ can be calculated as follows:

$$B_n(\alpha) = \int \sin\tilde{\gamma}\, f_O(\mathbf{u}) f_O(\mathbf{u}') \mathrm{d}\omega\, \mathrm{d}\omega', \tag{12}$$

where $\cos\tilde{\gamma} = \mathbf{u}\cdot\mathbf{u}'$ and $f_O(\mathbf{u})$ is the Onsager orientational distribution function [56], *i.e.*

$$f_O(\mathbf{u}) = \frac{\alpha}{4\pi \sinh\alpha} \cosh(\alpha \cos\theta), \tag{13}$$

where θ is the angle between the particle orientation $\mathbf{u}$ and the nematic axis and α is a non-negative parameter, which increases with increasing nematic order. Parameters ξ_1 and ξ_2 in eq. (11) are the same ones of eq. (10). We note that eqs. (10) and (11) have to be intended as manageable analytical expressions for theoretical calculations, which well reproduce the exact excluded volume in the isotropic and nematic phase, respectively. The degree of alignment in the system can also be quantified by the nematic order S, which is defined as the largest eigenvalue of the order matrix Q, *i.e.*:

$$Q_{\alpha\beta} = \frac{1}{N} \sum_i \frac{3}{2} \langle (\mathbf{u}_i)_\alpha (\mathbf{u}_i)_\beta \rangle - \frac{1}{2} \delta_{\alpha,\beta}, \tag{14}$$

where $\alpha\beta \in \{x, y, z\}$, and the unit vector $(\mathbf{u}_i(t))_\alpha$ is the component α of the orientation (*i.e.* the symmetry axis) of particle i at time t. A non-zero value of S signals the presence of the orientational order in the system. The parameter α is related to the nematic order parameter S as

$$S = \int_0^\pi \mathrm{d}\theta \sin\theta \left(\frac{3}{2}\cos^2\theta - \frac{1}{2}\right) f_O(\cos\theta) = 1 - 3\frac{\coth\alpha}{\alpha} + \frac{3}{\alpha^2} \xrightarrow{\text{high } \alpha} 1 - \frac{3}{\alpha}. \tag{15}$$

In the nematic phase all aggregates are assumed to possess an orientation which can be drawn from the same orientational distribution function independently of their length. Nevertheless, short aggregates are more likely isotropic than nematic and a proper correction term is added to the nematic free energy F as discussed in ref. [31]. Here, we evaluated this correction in eq. (6) by treating aggregates up to $l = 4$ as isotropic. A better approach would consist of introducing a chain-length–dependent Onsager parameter α, we plan to modify the theory along this direction in the future. A further improvement of the theory would be to employ a joint orientation and chain length distribution, as suggested first for non–self-assembling systems by van der Schoot and Cates [5]. A first attempt in this direction

[1] Except if two chains are constituted of two monomers.

has been done in ref. [30] and the present approach can be modified accordingly. Nevertheless, theoretical calculations would become rather demanding and cumbersome as well as, presumably, without a significant improvement in the accuracy of the theoretical predictions [30]. The free energy F depends solely on M in the istropic phase while it depends also on α in the nematic phase. By minimizing the free energy in the isotropic (nematic) phase with respect to M (M and α) for a given temperature and concentration, one obtains the equilibrium value of M (M and α). In ref. [55] it has been shown that assuming an exponential chain length distribution minimization of the free energy with respect to M leads to the following expression for the average chain length M_I in the isotropic phase:

$$M_I = \frac{1}{2}\left(1 + \sqrt{1 + 4\phi e^{k_I \phi \eta(\xi\phi) + \beta \Delta F_b}}\right), \qquad (16)$$

where ΔF_b is a parameter which depends on the free energy associated to the formation of a single bond [55]. Similarly, one obtains the following expression for the average chain length M_N in the nematic phase for long chains:

$$M_N = \frac{1}{2}\left(1 + \sqrt{1 + \alpha\phi e^{k_N(\alpha) \phi \eta(\xi\phi) + \beta \Delta F_b}}\right). \qquad (17)$$

Coexistence lines can be obtained by calculating the chemical potential and pressure in both I and N phase and by imposing that they have to be equal at coexistence. Finally, we note that in comparison with the theoretical treatment proposed in ref. [33] the present approach has been greatly simplified by considering an equivalent system of touching hard spheres both in the isotropic and nematic phases. Within the present approach one has to calculate the excluded volume between chains of bifunctional spheres just in the isotropic phase to estimate the parameters ξ_1 and ξ_2. In the nematic phase, assuming that an appropriate orientational distribution function is the Onsager function, the excluded volume can be calculated analytically.

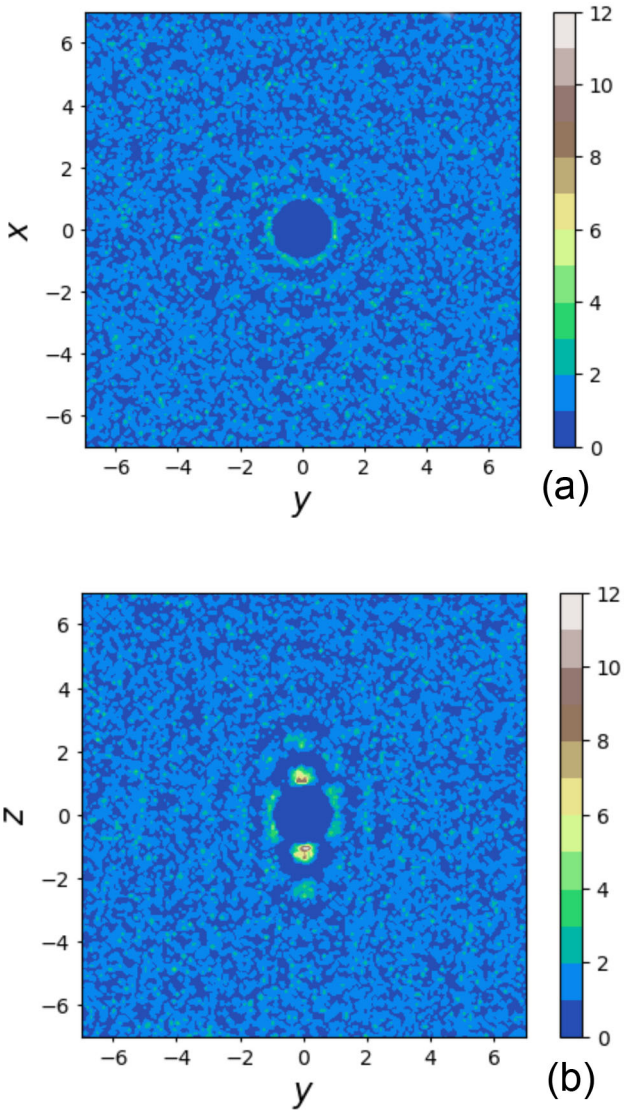

Fig. 2. Plot of $g(x, y, 0)$ (a) and $g(0, y, z)$ (b) where the z-axis is parallel to the nematic director for $T^* = 0.165$ and $\phi = 0.41$.

3 Results and discussion

3.1 Phase coexistence

We built the phase diagram for IN transition by calculating the probability distribution $P(N)$ of observing at coexistence N particles in the simulation box at fixed T and chemical potential as explained in sect. 2.2.

For nematic configurations we calculated the three-dimensional pair distribution function $g(\mathbf{r})$ defined as

$$g(\mathbf{r}) = \frac{1}{\rho N}\left\langle \sum_{i=1}^{N} \sum_{j \neq i} \delta(\mathbf{r} - (\mathbf{r}_i - \mathbf{r}_j)) \right\rangle, \qquad (18)$$

where $\delta(\mathbf{x})$ is the Dirac delta function. If the z-axis is chosen parallel to the nematic director, correlations in a plane perpendicular to the nematic director can be quantified by plotting $g(x, y, 0)$, while those in a plane parallel to it by plotting $g(0, y, z)$.

Figure 2 shows both $g(x, y, 0)$ and $g(0, y, z)$ for $T^* = 0.165$ and $\phi = 0.41$ and being representative of all simulations they show that no columnar, crystal or smectic phases are observed in our simulations.

The phase boundaries computed by simulation and theory are shown in fig. 3. It can be seen the KI provides very accurate results since the two SUS checkpoints at $T^* = 0.12$ and 0.155 coincide with the ones estimated by KI. Note that, as expected, the volume fractions of both the isotropic and nematic phases at coexistence increase on increasing T [31,33,44,55]. As already observed in refs. [33,34] theoretical predictions overestimate the extent of the coexistence region, although in the present case the coexistence region calculated by KI is significantly narrower than the one predicted theoretically. This result can be understood by calculating the order parameter S_l for

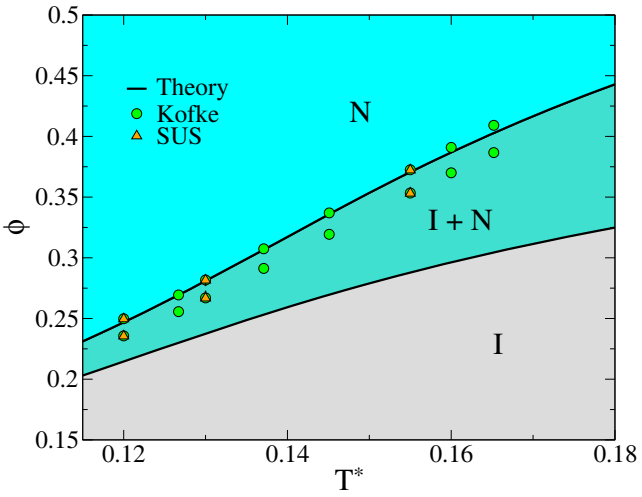

Fig. 3. Isotropic-nematic phase diagram in the packing-fraction ϕ *vs.* temperature T^* plane. Triangles are SUS simulations at $T^* = 0.12$, 0.130 and 0.155. Circles are results from the Kofke thermodynamic integration, started from the SUS simulation at $T^* = 0.130$. The other SUS simulations are used as checkpoints. Lines are obtained by theoretical calculations.

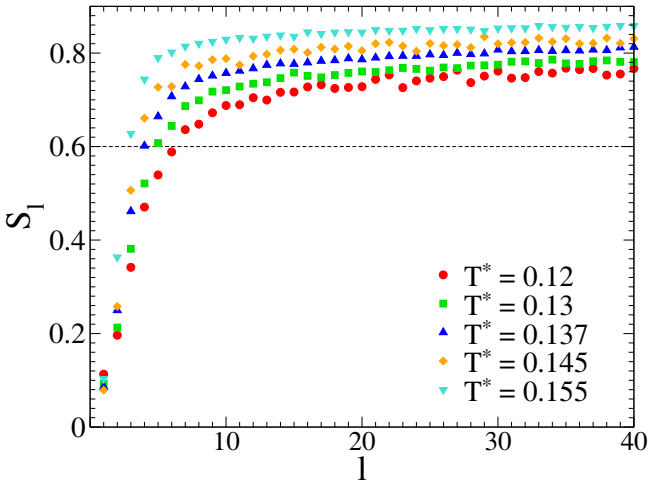

Fig. 4. Chain-length–dependent nematic order S_l in systems at different temperatures. Symbols are simulation data. The dashed line indicates $S = 0.6$.

individual clusters, which is estimated by evaluating the largest eigenvalue of the order tensor in eq. (14) calculated for all monomers belonging to clusters of size l [30]. Figure 4 shows S_l for several temperatures along the nematic coexistence line. It can be seen that aggregates of l up to 4–5 are more isotropic than nematic, a result which can ascribed to the lack of shape anisotropy of bifunctional KF spheres. Indeed, we remind that for hard cylinders of aspect ratio (*i.e.* the ratio of length over diameter) equal to 2, which have been studied in ref. [33], only monomers could be considered not nematic. Since theory does not account explicitly for such l-dependence of α, short chains are considered *as nematic as* long chains, thus favoring the nematic phase against the isotropic one and resulting in a wider coexistence region.

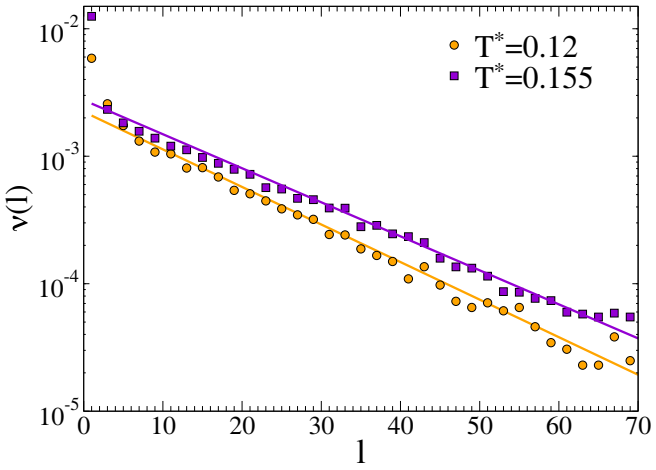

Fig. 5. Aggregate size distribution $\nu(l)$ for the nematic phase at coexistence for $T^* = 0.12$ and 0.155. Symbols are simulation data and lines are single exponential fits.

3.2 Cluster size distribution

One of the assumptions made in the theory illustrated in sect. 2.3 is that the cluster size distribution $\nu(l)$ is exponential. Figure 5 shows that a single exponential decay well describe $\nu(l)$ except for monomers. A different decay for small l can be ascribed to a different orientational ordering of smaller aggregates as evidenced by fig. 4. Short chains are more isotropic than long ones and the average chain length M in the isotropic phase is smaller than in the nematic phase, thus resulting in a faster decay of $\nu(l)$ for small l, since $\nu(l) \approx e^{-l/M}$. This behavior has been already observed in past studies [28,31,33] and as long as only short chains deviate from the exponential decay —as in the present case— the theoretical results are expected to be not significantly affected [31].

3.3 Reentrant behavior

Theoretical predictions for the coexisting volume fractions as a function of the average cluster size M are in agreement with numerical results obtained from NTV MC simulations as shown in fig. 6. The non-monotonic behavior of the nematic branch in fig. 6 is a distinctive feature of self-assembly–driven liquid crystals, since it cannot be accounted for by Onsager theory [33]. Nevertheless, to capture this reentrant behavior it is crucial to accurately calculate the excluded volume between polymers. Indeed, fig. 5(b) of ref. [33] shows the results predicted by Lu and Kindt's theory [28] and the one from the work of Kuriabova *et al.* [30] and, as in the Onsager theory, both these two approaches do not predict the reentrant behavior of the phase diagram in the ϕ-M plane.

Within the present theory the ratio $\mathcal{R}$ between the average chain length of the nematic phase M_N and that of the isotropic phase M_I at coexistence strongly depends on the packing fraction through an entropic contribution related to the orientational order in the system.

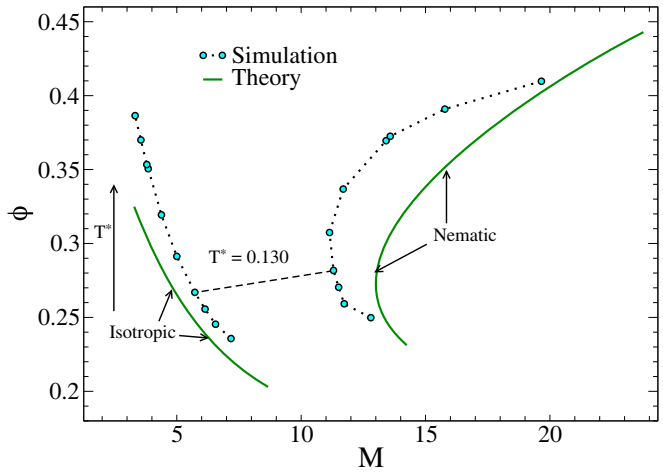

Fig. 6. Isotropic-nematic coexistence lines in the average length M and volume fraction ϕ-plane. Symbols are numerical results from NTV MC simulations. Solid lines are theoretical predictions and full circles along the isotropic and nematic phase boundaries, which are joined by dotted lines, indicate ϕ and M for isotropic and nematic phases at coexistence at the same temperature.

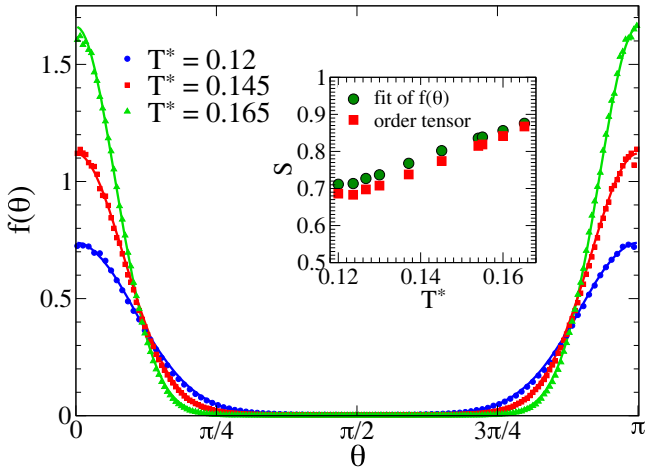

Fig. 7. Orientational distribution $f(\theta)$ from simulations (symbols) fitted to the Onsager trial function (solid lines) for $T^* = 0.12$, 0.145 and 0.165. Inset: values of the order parameter S obtained by fitting the simulation to the Onsager trial function (green circles) and as the largest eigenvalue of the order tensor (red squares).

At high temperatures nematization takes place at large ϕ and from eqs. (16) and (17) one has

$$\mathcal{R} = \frac{M_N}{M_I} \approx \sqrt{\alpha}. \tag{19}$$

Since the inverse of α controls the width of the orientational distribution of monomers, α is expected to increase dramatically at large ϕ, thus making $\mathcal{R}$ very large. Since at large volume fractions $M_I \approx 1$ [31], from eq. (19) it follows that M_N becomes very large too. Likewise, at low temperatures from eqs. (16) and (17) one has that [55]:

$$M_N \propto \sqrt{e^{\beta u_0}}, \tag{20}$$

thus increasing unbounded. According to the last two considerations we can argue that M_N can reasonably exhibit a minimum as a function of ϕ, *i.e.* it can exhibit a reentrant behavior as shown in fig. 6.

Finally, we remind that only the present theory is able to predict this reentrance in the M-ϕ plane compared to all other theoretical approaches (cf. ref. [33]) and actually this prediction still awaits experimental verification.

3.4 Orientational distribution function

In sect. 2.3 we also assumed that the distribution of orientations of aggregates in the nematic phase is well described by the Onsager trial function. Here, we would like to test this hypothesis since eq. (13) is known to work very well with non-assembling particles, such as hard spherocyinders [71] and ellipsoids [72–74], but it has not be assessed its validity in self-assembling systems yet. The fit of the Onsager trial function $f_O(\theta)$ to simulation data along the coexistence curve in the nematic phase is shown in fig. 7 and it can be clearly seen that it is able to well reproduce numerical data. Moreover, we calculated the order parameter S from the values of α obtained from the fits and we compare it with the values of S directly obtained by diagonalizing the order tensor as shown in the inset of fig. 7. The agreement between the two different estimates of the order parameter is rather satisfactory and suggests that the use of the Onsager trial function is a reasonable assumption in our theoretical treatment.

4 Conclusions

We studied a simple model of self-assembly–driven aggregation of patchy hard spheres and we reproduce the behavior already observed for other systems studied in the past such as patchy hard cylinder or patchy disks [31, 33, 44]. In particular, theoretical predictions for phase boundaries are in good agreement with data from MC simulations. The reentrant behavior in the elongation-concentration plane has been robustly confirmed and it can be considered a clear hallmark of the formation of self-assembly–driven liquid-crystalline phases, which still awaits for an experimental confirmation though. We also carefully checked the validity of an important hypothesis, which has been exploited in the theoretical approach, *i.e.* the assumption that the orientation of monomers can be described by the Onsager trial function.

Recent advances in the synthesis of patchy colloids of spherical shape [47] makes us confident that in the near future bifunctional spherical nanoparticles which self-assemble into linear chains of tunable stiffness will be available for experiments. Our numerical and theoretical approach is amenable to provide physical insight into these future experiments. For example, quantitative predictions on the dependence of phase boundaries on varying chain

flexibility can be easily obtained by the theory and compared with experimental findings. These novel colloidal liquid crystals with tunable physical properties are very promising candidates for bio and life science applications. For example their ability to transmit polarized light only at certain temperatures and concentrations could be exploited in medical diagnostics. More generally, patchy colloids can be envisaged as basic building blocks for creating materials with several applications. Many computer simulations have proved the emergence of unusual structures, such as Archimedian tilings [75] or diamond-like photonic crystals [76,77], in model colloidal systems which exhibit a full photonic bandgap. Reconfigurable materials based on soft, stimuli-responsive, patchy particles can be now fabricated and these materials can encode massive amounts of informations [78]. The possibility to induce the formation of a nematic phase on demand could provide a further flexibility in the design of these novel materials.

In conclusion, our work shows that with respect to isotropic and nematic phases reversible polymers made of spherical particles share the same properties of linear aggregates of anisotropic particles such as hard cylinders or disks. This finding was not *a priori* obvious due to the lack of shape anisotropy of monomers in the present system and provides a solid indication that the recent theoretical developments for these systems well capture the physics behind the formation of liquid-crystalline phases through self-assembly of both spherical and elongated building blocks into semi-flexible polymers.

Author contribution statement

All the authors were involved in the preparation of the manuscript. All the authors have read and approved the final manuscript.

References

1. I. Hamley, *Introduction to Soft Matter* (Wiley & Sons, 2007).
2. S.C. Glotzer, Science **306**, 419 (2004).
3. G.M. Whitesides, M. Boncheva, Proc. Natl. Acad. Sci. U.S.A. **99**, 4769 (2002).
4. A. Khan, Curr. Opin. Colloid Interface Sci. **1**, 614 (1996).
5. P. van der Schoot, M. Cates, Langmuir **10**, 670 (1994).
6. D.M. Kuntz, L.M. Walker, Soft Matter **4**, 286 (2008).
7. R. Mezzenga, J.M. Jung, J. Adamcik, Langmuir **26**, 10401 (2010).
8. C.F. Lee, Phys. Rev. E **80**, 031902 (2009).
9. A. Ciferri, Liq. Cryst. **34**, 693 (2007).
10. A. Aggeli, M. Bell, L.M. Carrick, C.W.G. Fishwick, R. Harding, P.J. Mawer, S.E. Radford, A.E. Strong, N. Boden, J. Am. Chem. Soc. **125**, 9619 (2003).
11. M. Nakata, G. Zanchetta, B.D. Chapman, C.D. Jones, J.O. Cross, R. Pindak, T. Bellini, N.A. Clark, Science **318**, 1276 (2007).
12. C. Maffeo, B. Luan, A. Aksimentiev, Nucl. Acids Res. **40**, 3812 (2012).
13. M. Salamonczyk, J. Zhang, G. Portale, C. Zhu, E. Kentzinger, J.T. Gleeson, A. Jakli, C. De Michele, J.K.G. Dhont, S. Sprunt *et al.*, Nat. Commun. **7**, 13358 (2016).
14. C. Robinson, Tetrahedron **13**, 219 (1961).
15. F. Livolant, A.M. Levelut, J. Doucet, J.P. Benoit, Nature **339**, 724 (1989).
16. K. Merchant, R.L. Rill, Biophys. J. **73**, 3154 (1997).
17. F. Tombolato, A. Ferrarini, J. Chem. Phys. **122**, 054908 (2005).
18. P. Mariani, F. Spinozzi, F. Federiconi, H. Amenitsch, L. Spindler, I. Drevensek-Olenik, J. Phys. Chem. B **113**, 7934 (2009).
19. F. Chami, M.R. Wilson, J. Am. Chem. Soc. **132**, 7794 (2010).
20. J. Lydon, Liq. Cryst. **38**, 1663 (2011).
21. P.K. Maiti, Y. Lansac, M.A. Glaser, N.A. Clark, Liq. Cryst. **29**, 619 (2002).
22. R.G. Edwards, J. Henderson, R.L. Pinning, Mol. Phys. **86**, 567 (1995).
23. J.R. Henderson, J. Chem. Phys. **113**, 5965 (2000).
24. K. Liu, Z. Nie, N. Zhao, W. Li, M. Rubinstein, E. Kumacheva, Science **329**, 197 (2010).
25. H.S. Park, S.W. Kang, L. Tortora, Y. Nastishin, D. Finotello, S. Kumar, O.D. Lavrentovich, J. Phys. Chem. B **112**, 16307 (2008).
26. N.B. Wilding, J. Phys.: Condens. Matter **9**, 585 (1996).
27. J. Herzfeld, Acc. Chem. Res. **29**, 31 (1996).
28. X. Lü, J.T. Kindt, J. Chem. Phys. **120**, 10328 (2004).
29. X. Lü, J. Kindt, J. Chem. Phys. **125**, 054909 (2006).
30. T. Kuriabova, M. Betterton, M. Glaser, J. Mater. Chem. **20**, 10366 (2010).
31. C. De Michele, T. Bellini, F. Sciortino, Macromolecules **45**, 1090 (2012).
32. M.M.C. Tortora, J.P.K. Doye, Mol. Phys. **116**, 2773 (2018).
33. K.T. Nguyen, F. Sciortino, C. De Michele, Langmuir **30**, 4814 (2014).
34. K.T. Nguyen, A. Battisti, D. Ancora, F. Sciortino, C. De Michele, Soft Matter **11**, 2934 (2015).
35. N. Kern, D. Frenkel, J. Chem. Phys. **118**, 9882 (2003).
36. M.S. Wertheim, J. Stat. Phys. **35**, 19 (1984).
37. M.S. Wertheim, J. Stat. Phys. **35**, 35 (1984).
38. M.S. Wertheim, J. Stat. Phys. **42**, 459 (1986).
39. M.S. Wertheim, J. Chem. Phys. **87**, 7323 (1987).
40. F. Sciortino, E. Bianchi, J.F. Douglas, P. Tartaglia, J. Chem. Phys. **126**, 194903 (2007).
41. E. Bianchi, J. Largo, P. Tartaglia, E. Zaccarelli, F. Sciortino, Phys. Rev. Lett. **97**, 168301 (2006).
42. F. Sciortino, J. Douglas, C. De Michele, J. Phys.: Condens. Matter **20**, 155101 (2008).
43. C. De Michele, G. Zanchetta, T. Bellini, E. Frezza, A. Ferrarini, ACS Macro Lett. **5**, 208 (2016).
44. E. Romani, A. Ferrarini, C. De Michele, Macromolecules **51**, 5409 (2018).
45. D.C. Williamson, G. Jackson, J. Chem. Phys. **108**, 10294 (1998).
46. R.M. Choueiri, E. Galati, H. Thérien-Aubin, A. Klinkova, E.M. Larin, A. Querejeta-Fernández, L. Han, H.L. Xin, O. Gang, E.B. Zhulina *et al.*, Nature **538**, 79 (2016).
47. S. Ravaine, E. Duguet, Curr. Opin. Colloid Interface Sci. **30**, 45 (2017).
48. G.R. Yi, D.J. Pine, S. Sacanna, J. Phys.: Condens. Matter **25**, 193101 (2013).

49. É. Duguet, C. Hubert, C. Chomette, A. Perro, S. Ravaine, C. R. Chim. **19**, 173 (2016).
50. H. Bao, T. Bihr, A.S. Smith, R.N. Klupp Taylor, Nanoscale **6**, 3954 (2014).
51. A.A. Shah, B. Schultz, K.L. Kohlstedt, S.C. Glotzer, M.J. Solomon, Langmuir **29**, 4688 (2013).
52. C.M. Rachelle, E. Galati, A. Klinkova, H. Therien-Aubin, E. Kumacheva, Faraday Discuss. **191**, 189 (2016).
53. Y. Zhao, R. Berger, K. Landfester, D. Crespy, Polym. Chem. **5**, 365 (2014).
54. C. Bae, H. Kim, J.M. Montero Moreno, G.R. Yi, H. Shin, Sci. Rep. **5**, 9339 (2015).
55. C. De Michele, L. Rovigatti, T. Bellini, F. Sciortino, Soft Matter **8**, 8388 (2012).
56. L. Onsager, Ann. N.Y. Acad. Sci. **51**, 627 (1949).
57. T. Odijk, Macromolecules **19**, 2313 (1986).
58. G.J. Vroege, H.N.W. Lekkerkerker, Rep. Prog. Phys. **55**, 1241 (1992).
59. J.R. Henderson, Phys. Rev. Lett. **77**, 2316 (1996).
60. J.R. Henderson, Phys. Rev. E **55**, 5731 (1997).
61. C. Vega, E. Sanz, J.L.F. Abascal, E.G. Noya, J. Phys.: Condens. Matter **20**, 153101 (2008).
62. D.A. Kofke, J. Chem. Phys. **98**, 4149 (1993).
63. P. Tian, D. Bedrov, G.D. Smith, M. Glaser, J. Chem. Phys. **115**, 9055 (2001).
64. P. Virnau, M. Muller, J. Chem. Phys. **120**, 10925 (2004).
65. R.L.C. Vink, T. Schilling, Phys. Rev. E **71**, 051716 (2005).
66. J.D. Parsons, Phys. Rev. A **19**, 1225 (1979).
67. S. Lee, J. Chem. Phys. **87**, 4972 (1987).
68. S. Varga, I. Szalai, Mol. Phys. **98**, 693 (2000).
69. D.A. McQuarrie, *Statistical Mechanics* (University Science Books, Sausalito, CA, 2000).
70. D.C. Williamson, G. Jackson, Mol. Phys. **86**, 819 (1995).
71. S.C. McGrother, D.C. Williamson, G. Jackson, J. Chem. Phys. **104**, 6755 (1996).
72. D. Frenkel, B.M. Mulder, J.P. McTague, Phys. Rev. Lett. **52**, 287 (1984).
73. M. Allen, D. Frenkel, J. Talbot, Comput. Phys. Rep. **9**, 301 (1989).
74. M.P. Allen, G. Evans, D. Frenkel, B.M. Mulder, Adv. Chem. Phys. **86**, 1 (1993).
75. S. Whitelam, Phys. Rev. Lett. **117**, 228003 (2016).
76. F. Smallenburg, F. Sciortino, Nat. Phys. **9**, 554 (2013).
77. F. Romano, F. Sciortino, Nat. Commun. **3**, 975 (2012).
78. C.L. Phillips, E. Jankowski, B.J. Krishnatreya, K.V. Edmond, S. Sacanna, D.G. Grier, D.J. Pine, S.C. Glotzer, Soft Matter **10**, 7468 (2014).